www.ietdl.org

Published in IET Image Processing
Received on 10th July 2013
Revised on 15th July 2014
Accepted on 26th August 2014
doi: 10.1049/iet-ipr.2013.0501

ISSN 1751-9659

Content-based image retrieval in dermatology using intelligent technique

Gnanasigamony Wiselin Jiji, Peter Savariraj Johnson Durai Raj

Department of CSE, Dr. Sivanthi Aditanar College of Engineering, Tiruchendur-628215, Tamilnadu, India
E-mail: jijivevin@yahoo.co.in

Abstract: This study proposes a content-based image retrieval system for skin lesion images as a diagnostic aid. Effectiveness is measured by the rate of correct retrieval of images from skin lesions. The proposed architecture is used to retrieve digital images and the name of the disease category from an image data repository by the contents in the image, such as shape, texture and colour that is extracted from the image. The author's proposed algorithm used feature vector, classification and regression tree to retrieve comprehensive reference sources for diagnostic purpose. The results proved using a receiver operating characteristic curve that the proposed architecture has high contribute to computer-aided diagnosis of skin lesions. Experiments on a set of 1210 images yielded a specificity of 97.25% and a sensitivity of 91.24%. Their empirical evaluation has a superior retrieval and diagnosis performance when compared to the performance of other works. The authors present explicit combinations of feature vectors corresponding to healthy and lesion skin.

1 Introduction

Dermatologists base the diagnosis of skin disease on the visual assessment of the skin. This fact shows that correct diagnosis is highly dependent on the observer's experience and on his or her visual perception. Moreover, the human vision system lacks accuracy, reproducibility and quantification in the way it gathers information from an image. So, there is a great need for computer-aided diagnosis.

Content-based image retrieval (CBIR) refers to the retrieval of images from a database that are related to a query image, using measures of information derived from the images themselves, rather than relying on the accompanying text or annotation [1]. The potential feature descriptors of image content relates to colour, texture, shape or spatial relationship. Colour has proven to be an effective descriptor regarding skin [2], especially in dermatology. In [3, 4], it was shown that the representation of an image in terms of colour differences between lesion and healthy skin is advantageous over the use of the combined colour features.

The major contributions considered in this work are:

- The work concentrated on 20 different skin lesions.
- Retrieved images of similar diseases that lead to similar diagnosis of the input image.
- Guide the physician by predicting the disease of a particular case and to assist them in diagnosis.

First, after examining the skin images, pre-processing will be performed. Second, we examine the visual features of skin disease classified in the database and select colour, texture and shape for characterisation of a certain skin disease. Third, feature extraction techniques for each visual feature are investigated, respectively, and feature selection is carried out. Fourth, retrieval system based on the extracted features will be discussed. The experimental data set is divided into two parts: developmental data set used as an image library and an unlabelled independent test data set. Two sets of experiments are performed: the input image of the skin image retrieval algorithm is either from the developmental data set or independent test data set. Effectiveness is measured by the rate of correct retrieval of images from 20 classes of skin lesions. We employ and compared two different methods to learn favourable feature representations for this special application.

2 Related research

Claridge *et al.* [5] described an automated method of extracting the irregularity in shape or outline of a mole. They used features expressed by 'bulkiness' measure and irregularity of the border is expressed by 'structural' aspect of the shape and the other for the 'textural' aspect. Their method has a specificity of 69% and a sensitivity of 91% compared with, respectively, 89 and 48% for the average dermatologist. Stoecker *et al.* [6] gave an overview of the surge in digital imaging in dermatology that happened at that time, and described the potential benefits. They concluded that in 1992, no one really knew the answer to whether or not diagnoses could be automatically acquired from images, and notes that any approach that mimics dermatologists is likely to have severe limitations, as dermatologists are about 75% accurate in their diagnoses and often unable to explain how they come to a diagnosis.

Celebi *et al.* [7] presented a systematic overview of recent border detection methods: clustering followed by active

contours are the most popular. Numerous features have been extracted from skin images, including shape, colour, texture and border properties [8, 9]. Classification methods range from discriminant analysis to neural networks and support vector machines [10]. These methods are mainly developed for images acquired by epiluminescence microscopy (ELM or dermoscopy) and they focused on melanoma, which is rare, but quite dangerous condition. Chung and Wang [11] created a skin cancer database. The query as an image is processed based on data mining to obtain the images which are similar to that. Celebi and Aslandogan [12] developed a system for retrieving skin lesion images based on shape similarity. Results on 184 skin lesion images show significant agreement between computer assessment and human perception. However, they only focus on silhouette shape similarity and do not include many features (colour and texture) described in other papers by the same authors [10]. Rahman *et al.* [13] presented a CBIR system for dermatoscopic images. Their approach includes image processing, segmentation, feature extraction (colour and textures) and similarity matching. Experiments on 358 images of pigmented skin lesions from three categories (benign, dysplastic nevi and melanoma) are performed. A quantitative evaluation based on the precision curve shows the effectiveness of their system to retrieve visually similar lesions (average precision 60%). Dorileo *et al.* [14] presented a CBIR system for wound images (necrotic tissue, fibrin, granulation and mixed tissue). Features based on histogram and multispectral co-occurrence matrices are used to retrieve similar images. The performance is evaluated based on measurements of precision (50%) on a database of 215 images. All these approaches only consider a few classes of lesions and/or do not exploit many useful features in this context. Dermatology atlases containing a large number of images are available online [15, 16]. However, their searching tool only allows query by the name of the lesion. On the other hand, the possibility of retrieving images based on visual similarity would greatly benefit both the non-expert users and the dermatologists. As already pointed out [13], there is a need for CBIR as a decision support tool for dermatologists in the form of a display of relevant past cases, along with proven pathology and other suitable information. CBIR could be used to present cases that are not only similar in diagnosis, but also similar in appearance and cases with visual similarity but different diagnoses.

The 'ultimate goal' of this work is an automated diagnostic assistant with a large database of images which is capable of suggesting possible diagnoses and showing similar images to help a physician make a diagnosis.

3 Our work

A practical approach to the retrieval of dermoscopy images is presented. Fig. 1 shows an overview of the proposed approach. Initially 66 feature vectors are used extracted from skin images and applying dimensionality reduction, we selected most promising 20 feature vectors using 'Scree Graph'. Finally, we have implemented a fusion strategy colour and texture and shape feature vectors for image retrieval system using decision tree – classification and regression tree (CART) [17, 18].

3.1 Data set description

The digital dermoscopy images and its symptoms treatment plans and case histories are collected from Government Medical College, Tirunelveli, India and some of online repositories http://www.library.med.utah.edu, http://www.medicinenet.com. These were annotated by Dr. Sathish Kumar, professional dermatologists. There are 20 classes with 1210 colour images in resolution of 768 × 512 pixels. Fig. 2 shows sample images along with diagnosed diseases.

3.2 Border detection

The first step in the computerised analysis of skin lesion images is the detection of the lesion borders. The importance of the border detection for the analysis is 2-fold. Firstly, the border structure provides vital information for accurate diagnosis. Secondly, the extraction of other important colour or texture related clinical features critically depends on the accuracy of the border detection.

For border detection, an automated method level set evolution without re-initialisation [19] is used. It has the following advantages:

- No re-initialisation, implementation is consistent.
- Allows large time step, faster curve evolution.
- Flexible and efficient initialisation.
- Very simple numerical scheme and easy implementation.

The border detection method was applied to all images.

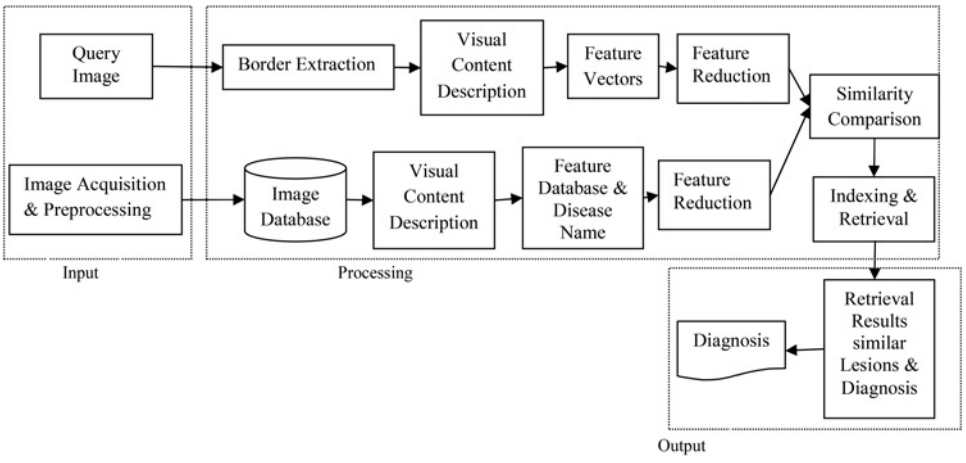

Fig. 1 *Proposed architecture*

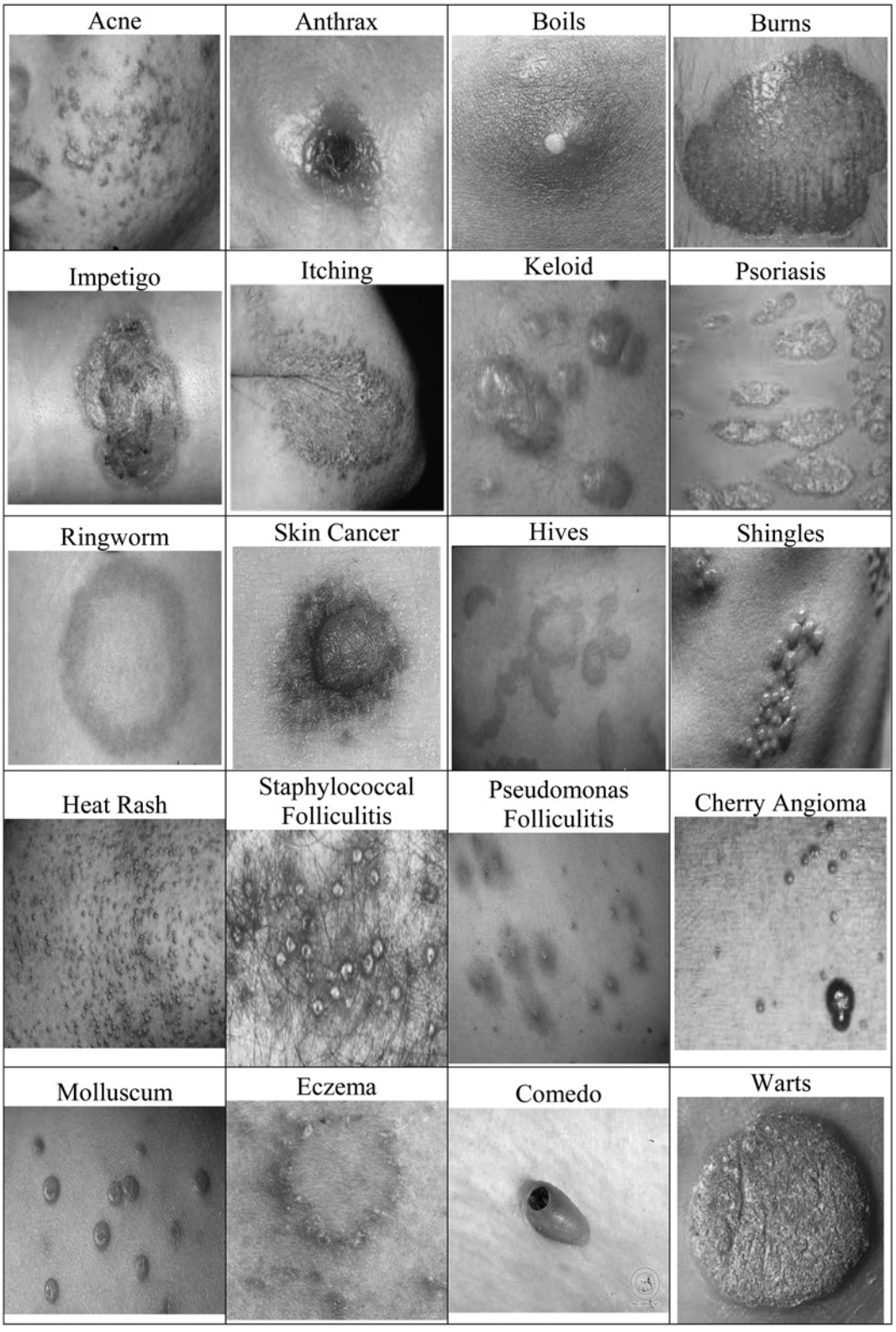

Fig. 2 *Sample images used in our work*

3.3 Feature extraction

Prior to retrieval system, texture, shape and colour features are extracted from the image to capture descriptive feature information. CART is used for grouping of similar pattern diseases. In this section, the features that were used to characterise the skin lesion images are described.

3.3.1 Description of the shape features: Shape is an important clinical feature in the diagnosis of pigmented skin lesions.

(a) *Bending energy:* It is calculated through the curvature of the boundary at each point. Let $x(i)$ and $y(i)$ be the ith

doi: 10.1049/iet-ipr.2013.0501

coordinate location describing an object's boundary. Then the curvature of this boundary at the ith position is defined as

$$C(i)^2 = (2*x(i) - x(i-1) - x(i+1))^2 + (2*y(i) - y(i-1) - y(i+1))^2 \quad (1.a)$$

where $i \in [1, M–2]$ and M is the number of points on the boundary.

Curvature normalised with boundary length P is called the bending energy

$$E = (1/P)* \sum_{i=1}^{M-2} C(i)^2 \quad (1.b)$$

(b) *Contour moments:* Let $z(i)$ be an ordered sequence that represents the Euclidean distance between the centroid and all N boundary pixels of the object. The rth contour sequence moment m_r and the rth central moment μ_r can be defined as the following equations

$$m_r = (1/N) \times \sum_{i=1}^{N} [z(i)]^r \quad (2)$$

$$\mu_r = (1/N) \times \sum_{i=1}^{N} [z(i) - m_1]^r \quad (3)$$

(c) *Invariant moments (order 1–3):* Moment invariants are calculated as follows (see (4))

where $\eta_{ij} = \mu_{ij}/\mu_{00}^{(1+((i+j)/2))}$ and μ_{ij} is the $(i+j)$th central moment defined in (3).

(d) *Area (A):* The lesion area can be calculated by counting the number of pixels inside the border. The perimeter of a lesion is calculated by counting the number of pixels on the boundary.

(e) *Compactness*: While area and perimeter are both invariant with respect to translation and rotation, they are not invariant to scaling. A combination of both descriptors could be used to obtain a dimensionless measurement which is invariant to translation, rotation and scaling. Compactness is defined as follows

$$4*\pi*\text{Area}/\text{Perimeter}^2 \quad (5)$$

which is a measure of the roundness of a shape and is minimal for a circular shape [20]. Objects having irregular boundaries have larger compactness.

(f) *Aspect ratio*: It can be defined as the ratio of the length of the major axis ($L1$) to the length of the minor axis ($L2$). Here, (r_0, c_0) denotes the object centroid, and m_{pq} and μ_{pq} denote the $(p+q)$th order geometric and central moments of the object. It is given in Table 1.

(g) *Asymmetry*: Asymmetry [21] ($A1$ and $A2$) is evaluated as follows: first, the major axis orientation of the object (θ) was calculated. Second, the object was rotated θ degrees clockwise to align the principal axes with the image x and y axes. The object was then hypothetically folded about the x-axis and the area difference (Ax) between the overlapping folds was taken as the amount of asymmetry about the x-axis. The same procedure was performed for the y-axis. Two asymmetry measures were calculated from Ax and Ay as shown in Table 1.

(h) *Eccentricity*: Eccentricity of an object can be defined as lines that intersect orthogonally at the centroid of the object and represent the directions with zero cross correlation. Eccentricity is defined as

$$\varepsilon = \frac{(\mu_{02} - \mu_{20})^2 + 4\mu_{11}}{(\mu_{02} - \mu_{20})^2} \quad (6)$$

(i) *Convex area and perimeter*: A vital class of shape representation methods is based on defining a bounding region that encloses the shape of interest. The convex hull is defined as the smallest convex set that contains the shape. Convex hull is computed using the Graham Scan [22]. The area of the convex hull is computed by selecting an arbitrary point inside the hull. In this work, centroid is

Table 1 Formulae for shape features used

Aspect ratio	Asymmetry
$m_{pq} = \sum_{i=0}^{\text{rows}} \sum_{j=0}^{\text{cols}} i^p j^q$	$\theta = \frac{1}{2}\tan^{-1}\left(\frac{2\mu_{11}}{\mu_{20} - \mu_{02}}\right)$
$r_0, c_0 = (m_{10}/m_{00}, m_{01}/m_{00})$	$A_1 = \frac{\min(A_x, A_y)}{A} \times 100\%$
$\mu_{pq} = \sum_{i=0}^{\text{rows}} \sum_{j=0}^{\text{cols}} (i - r_0)^p \cdot (j - c_0)^q$	$A_2 = \frac{A_x + A_y}{A} \times 100\%$
$L_{1,2} = (8(\mu_{02} + \mu_{20} \pm ((\mu_{02} - \mu_{20})^2 + 4\mu_{11})^{1/2}))^{1/2}$	
$A_{R=L_1/L_2}$	

$$\begin{aligned}
I_1 &= \eta_{20} + \eta_{02} \\
I_2 &= (\eta_{20} + \eta_{02})^2 + (2\eta_{11})^2 \\
I_3 &= (\eta_{30} - 3\eta_{12})^2 + (3\eta_{21} - \eta_{03})^2 \\
I_4 &= (\eta_{30} + \eta_{12})^2 + (\eta_{21} + \eta_{03})^2 \\
I_5 &= (\eta_{30} - 3\eta_{12})(\eta_{30} + \eta_{12})[(\eta_{30} + \eta_{12})^2 - 3(\eta_{21} + \eta_{03})^2] \\
&\quad + (3\eta_{21} - \eta_{03})(\eta_{21} + \eta_{03})[3(\eta_{30} + \eta_{12})^2 - (\eta_{21} + \eta_{03})^2] \\
I_6 &= (\eta_{20} - \eta_{02})[(\eta_{30} + \eta_{12})^2 - (\eta_{21} + \eta_{03})^2] + 4\eta_{11}(\eta_{30} + \eta_{12})(\eta_{21} + \eta_{03}) \\
I_7 &= (3\eta_{21} - \eta_{03})(\eta_{30} + \eta_{12})[(\eta_{30} + \eta_{12})^2 - 3(\eta_{21} + \eta_{03})^2] \\
&\quad - (\eta_{30} - 3\eta_{12})(\eta_{21} + \eta_{03})[3(\eta_{30} + \eta_{12})^2 - (\eta_{21} + \eta_{03})^2]
\end{aligned} \quad (4)$$

selected. The hull perimeter is calculated by summing the Euclidean distances between adjacent points in the hull.
(j) *Convexity*: It is the relative amount that an object differs from a convex object [23]. It is formulated as the ratio of the perimeter of a convex hull of an object to the perimeter of the object. It is equal to 1 for convex objects. Objects having irregular boundaries have convexity less than 1.
(k) *Solidity*: It measures the density of an object and is defined as the ratio of the area of an object to the area of a convex hull of the object [23]. Objects having irregular boundaries have solidity less than 1.

3.3.2 Description of the texture features: (a) *Busyness*: A busy texture is one in which there are rapid changes of intensities from one pixel to its neighbour. The spatial frequency of intensity changes reflects the level of busyness, the magnitude of these changes depend upon the dynamic range of grey scale and thus relates to contrast. The busyness by Amadasun and King [24] is represented as follows

$$f_{\text{bus}} = \frac{\left[\sum_{i=0}^{G_h} p_i s(i)\right]}{\left[\sum_{i=0}^{G_h}\sum_{j=0}^{G_h} ip_i - jp_j\right]}, \quad p_i \neq 0, p_j \neq 0 \tag{7}$$

where the numerator is essentially a measure of the spatial rate of change in intensity and the denominator is the summation of the magnitude of difference between the different grey-tone values. p_i is the probability of occurrence of grey-tone value I which is given by, $P_1 = N_i/n^2$, where $n = N–2d$, where d specifies the neighbourhood size $s(i)$ is ith entry in the neighbourhood grey-tone difference matrix which is given by

$$\begin{aligned} s(i) &= \sum |i - \overline{A_i}|, \quad \text{for} \quad i \in N_i \quad \text{if} \quad N_i \neq 0 \\ &= 0, \qquad\qquad \text{otherwise} \end{aligned} \tag{8}$$

where A_i is the average grey-tone over the neighbourhood. It is represented as

$$\overline{A_i} = \overline{A}(k, l) = \frac{1}{W-1}\left[\sum_{m=-d}^{d}\sum_{n=-d}^{d} f(k+m, l+n)\right], \quad (m, n) \neq (0, 0) \tag{9}$$

(b) *Colour texture spectrum*: Jiji [25] developed an efficient feature colour texture spectrum to extract the texture property of images, which is illustrated in Fig. 3.

3.3.3 Description of the colour features: Colour space, colour quantification and similarity measurement are the key components of colour feature extraction.

(a) *Colour statistics*: Mean + Std + moments: Various combinations of colour statics obtained the best results by combining mean, standard deviation and moments from degree 2 to 5 for each channel in the RGB and *L*a*b** spaces. The moment of degree 'n' for a spectral dimension 'h' is defined by López *et al.* [26] is as follows

$$M_n(C_h) = \sum_{j=1}^{N}\left(C_{hj} - \mu_{C_h}\right)^n p(C_{hj}) \tag{10}$$

where C_h is the random variable, $p(C_{hj})$, $j = 1, 2, \ldots, N$ is the histogram, N is the number of distinct variable values, which has been estimated through a 256-bin histogram and μ_{C_h} is the mean value of C_h. We used standardised moments to avoid the non-dimensional, so (10) is divided by $\sigma_{c_h}^n$ where σ_{c_h} is the standard deviation of c_h.
(b) *Co-occurrence of colour indices:* It is a co-occurrence matrix calculated by the image colour values. By use of uniform partition of the RGB space, we compute eight co-occurrence matrices corresponding to the following

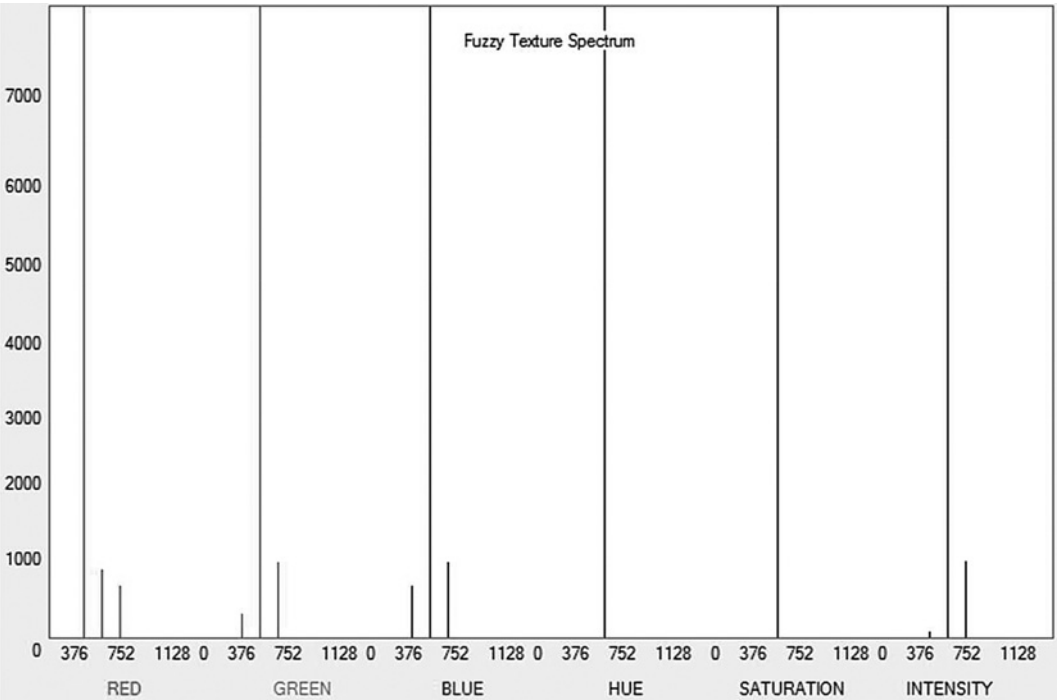

Fig. 3 *Colour fuzzy texture spectrum for the image Fig. 8a*

doi: 10.1049/iet-ipr.2013.0501

displacement vectors: {(1,0), (1,1), (0,1), (−1,1), (−1,0), (−1, −1), (0, −1) and (1, −1)}. The matrices are averaged for rotation invariance, and the following five features are computed as in [27, 28].

Contrast

$$\mathrm{CN} = \frac{1}{(G-1)^2}\sum_{u=0}^{G-1}\sum_{v=0}^{G-1}|u-v|^2 p(u,v) \tag{11}$$

Correlation

$$\mathrm{CR} = \frac{1}{2}\sum_{u=0}^{G-1}\sum_{v=0}^{G-1}\frac{(u-\mu_u)(v-\mu_v)}{\sigma_u^2\sigma_v^2}p(u,v)+1 \tag{12}$$

Entropy

$$\mathrm{ET} = -\frac{1}{2\log(G)}\sum_{u=0}^{G-1}\sum_{v=0}^{G-1}p(u,v)\log_2[p(u,v)] \tag{13}$$

Energy

$$\mathrm{EN} = \sum_{u=0}^{G-1}\sum_{v=0}^{G-1}p(u,v)^2 \tag{14}$$

Homogeneity

$$\mathrm{HM} = \sum_{u=0}^{G-1}\sum_{v=0}^{G-1}\frac{p(u,v)}{1+|u-v|} \tag{15}$$

where u and v are the coordinates of the co-occurrence matrix, G is the number of grey levels, μ_u, μ_v, σ_u and σ_v are the mean values and the standard deviations of the uth row of the vth column of the co-occurrence matrix, respectively.

3.4 Feature selection

This is an important step to reduce the dimensionality of the feature space by filtering approach. Mathematical theory stated that 'variance determines the spread of a distribution and high variance indicates that the data points are very spread out from each other [29]' and is carried out in three phases.

1. In the first phase, we calculated the variance within class for each feature vectors and is given below.

$$\begin{aligned}&\text{For each } c = 1, \ldots, C;\ i = 1, \ldots, N,\\ &X_{c,i} = \{x_{c,i,j}{:}j = 1, \ldots, S\}\end{aligned} \tag{16}$$

where C is the number of classes, N is the number of features and S is the number of samples in each class

$$V_{c,i} = \mathrm{var}(X_{c,i}), \quad c = 1, \ldots, C;\ i = 1, \ldots, N \tag{17}$$

where $\mathrm{var}(X_{c,i})$ denotes the variance of $X_{c,i}$

$$V_i = \frac{\sum_{c=1}^{C} V_{c,i}}{C}, \quad i = 1, \ldots, N \tag{18}$$

2. In the second phase, we calculated variance among all classes for each feature vector and is given in (19) and (20).

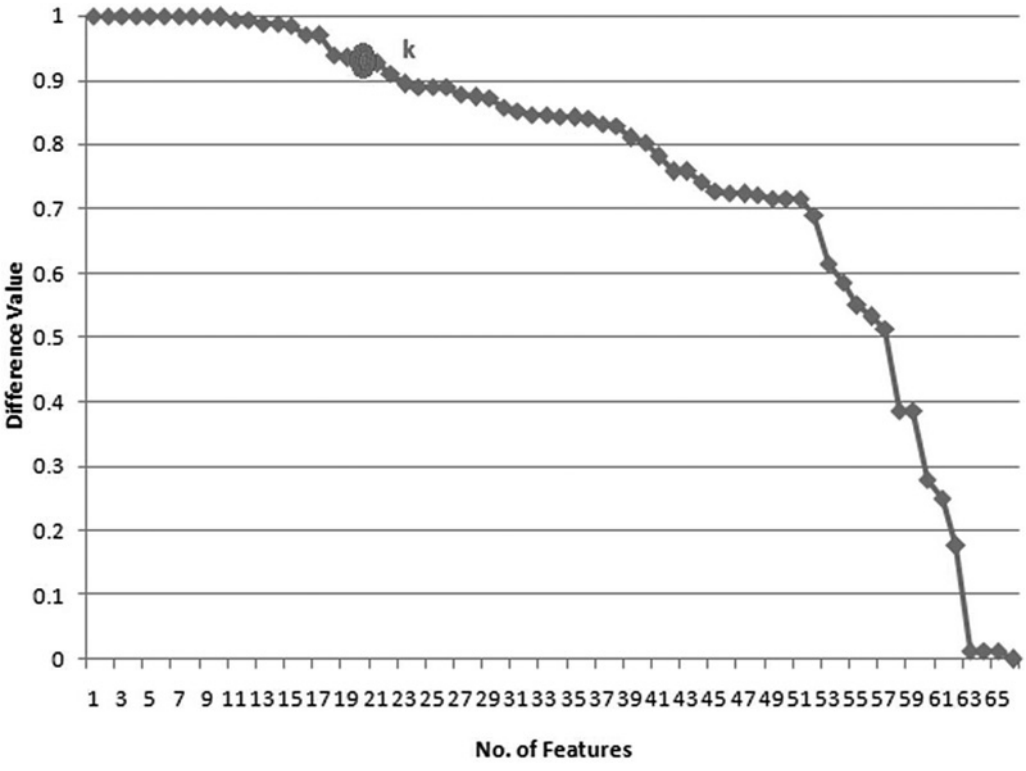

Fig. 4 *Scree graph*

For each $i = 1, \ldots, N$

$$X_i = \bigcup_{c=}^{C} X_{c,i} \tag{19}$$

$$V^{(i)} = \text{var}(X_i), \quad i = 1, \ldots, N \tag{20}$$

1. Calculated the difference between average variance of classes and variance values obtained in Phase 2 and is given in (21). Differences values are sorted in the descending order

$$D_i = \left| V^{(i)} - V_i \right|, \quad i = 1, \ldots, N \tag{21}$$

A 'Scree' graph is plotted against number of features against and values in Phase 3 and is given in Fig. 4. Select the peak of the graph and mark the drop position 'k'. The features selected are steep to the left and not steep to the right of 'k'. The selected features are busyness, invariant moment (order 1, 3), area, aspect ratio, compactness, eccentricity, asymmetry (both major axis), convex area, convexity, solidity, contrast, correlation, entropy, colour statistics – mean, standard deviation and moment.

3.5 Retrieval system

The leaf nodes denote the category of classes. The tree is built recursively, starting from the root node. In our work, CART – decision tree inducer [17, 18] is used for building decision tree. Let t_p be a parent node and t_l, t_r be the right and left nodes, respectively. $x_j \le x_j^R$ is the best splitting rule of variable x_j, $j = 1, \ldots, M$. M is the total number of selected features. x_j^R is the best splitting value of x_j. The impurity of the node is defined by impurity function $i(t)$ where t denotes the current node. Change of impurity function $\Delta i(t)$

$$\Delta i(t) = i(t_p) - E[i(t_c)] \tag{22}$$

where t_c is the left and right child nodes of the parent node t_p. Assume that P_l and P_r are the probability of the left and right nodes, we obtain

$$\Delta i(t) = i(t_p) - P_l i(t_l) - P_r i(t_r) \tag{23}$$

At each node CART solves the maximisation problem as follows

$$\underset{x_j \le x_j^R,\, j=1,..,M}{\arg\max} \quad [i(t_p) - P_l i(t_l) - P_r i(t_r)] \tag{24}$$

From (24), the CART search through the all possible values of all variables in matrix $\boldsymbol{M}$ for the best splitting rule $x_j \le x_j^R$ which will maximise the change of impurity measure.

In our method, the Gini index is used as $i(t)$. So the impurity function defined as

$$i(t) = \sum_{k \ne l} p(k|t)p(l|t) \tag{25}$$

where $k, l, \quad 1, \ldots, C$ is the index of the class; $p(k|t)$ is the conditional probability of the class k provided the current node t.

Table 2 Statistical performance analysis for different distance measures

Class	Euclidean [31]				Mahanalobis [30]				Chebyshev [32]			
	Accuracy	Sensitivity	Specificity	*F*-measure	Accuracy	Sensitivity	Specificity	*F*-measure	Accuracy	Sensitivity	Specificity	*F*-measure
1	0.949	0.990	0.988	0.947	0.950	0.700	0.977	0.736	0.950	0.700	0.977	0.736
2	0.962	0.900	0.966	0.818	0.840	0.500	0.877	0.384	0.860	0.600	0.888	0.461
3	0.965	0.600	0.990	0.747	0.950	0.800	0.966	0.761	0.960	0.800	0.966	0.761
4	0.985	0.999	0.990	0.990	0.980	0.800	0.999	0.888	0.980	0.800	0.999	0.888
5	0.938	0.900	0.988	0.900	0.940	0.700	0.966	0.700	0.940	0.700	0.966	0.700
6	0.954	0.990	0.990	0.990	0.920	0.800	0.933	0.746	0.900	0.700	0.922	0.946
7	0.949	0.900	0.988	0.900	0.940	0.400	0.999	0.551	0.940	0.400	0.999	0.528
8	0.968	0.900	0.988	0.942	0.940	0.700	0.966	0.700	0.960	0.800	0.977	0.800
9	0.982	0.990	0.977	0.904	0.970	0.800	0.988	0.841	0.950	0.700	0.977	0.736
10	0.939	0.900	0.988	0.900	0.960	0.800	0.988	0.841	0.950	0.700	0.977	0.736
11	0.934	0.980	0.977	0.921	0.920	0.700	0.966	0.781	0.924	0.600	0.220	0.750
12	0.951	0.970	0.966	0.853	0.921	0.900	0.955	0.812	0.918	0.800	0.933	0.684
13	0.928	0.900	0.955	0.849	0.934	0.700	0.899	0.785	0.831	0.700	0.911	0.781
14	0.952	0.940	0.990	0.793	0.901	0.800	0.922	0.725	0.901	0.900	0.900	0.621
15	0.961	0.700	0.900	0.716	0.919	0.800	0.944	0.845	0.896	0.600	0.911	0.812
16	0.949	0.900	0.922	0.928	0.901	0.900	0.999	0.912	0.890	0.800	0.923	0.912
17	0.957	0.990	0.988	0.946	0.875	0.700	0.922	0.715	0.912	0.600	0.944	0.823
18	0.968	0.980	0.990	0.891	0.892	0.800	0.912	0.729	0.921	0.800	0.910	0.816
19	0.939	0.900	0.922	0.900	0.905	0.700	0.988	0.651	0.886	0.900	0.931	0.712
20	0.946	0.920	0.988	0.923	0.942	0.900	0.911	0.700	0.871	0.700	0.901	0.541

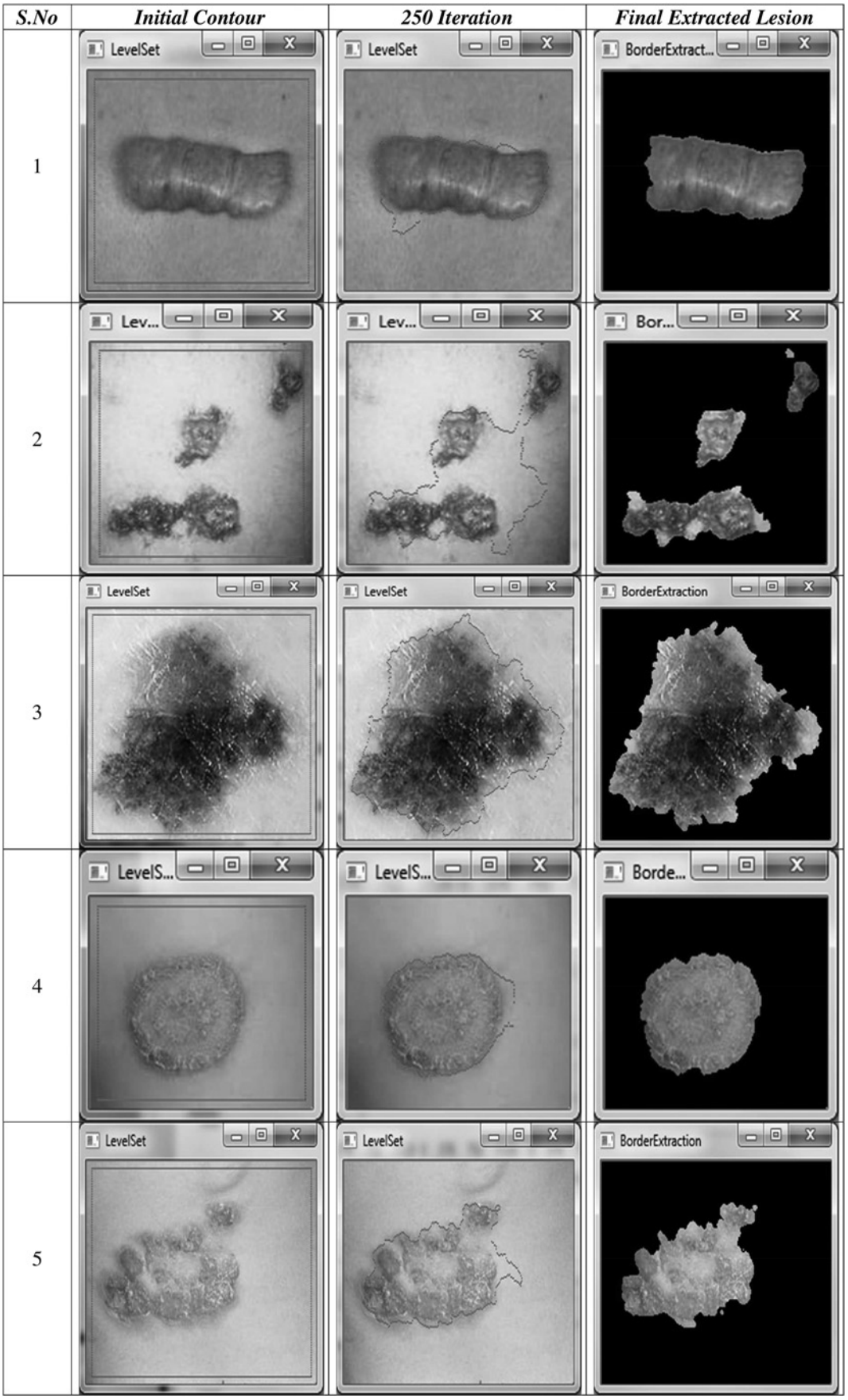

Fig. 5 *Sample output results for border detection*

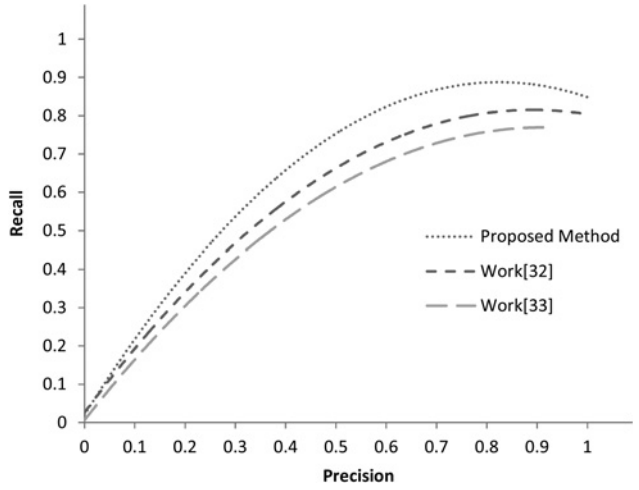

Fig. 6 *Precision recall analysis for proposed method with work [33, 34]*

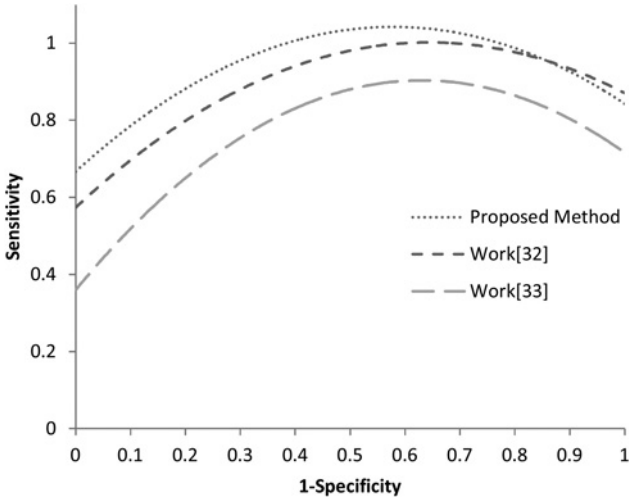

Fig. 7 *ROC analysis for proposed method with work [33, 34]*

By applying the Gini index for the above maximisation problem in (24) we will obtain

$$\underset{x_j \le x_j^R, j=1,..,M}{\arg\max} \left[-\sum_{k=1}^{K} p^2(k|t_p) + P_l \sum_{k=1}^{K} p^2(k|t_l) + P_r \sum_{k=1}^{K} p^2(k|t_r) \right] \tag{26}$$

So that in each node is framed with an attribute and the splitting rule.

After the tree is built will be pruned with the K-fold cross validation. In our experiment the $k = 10$. The misclassification error is calculated for estimate the cost of the tree. And the tree may differ from time to time because the training and

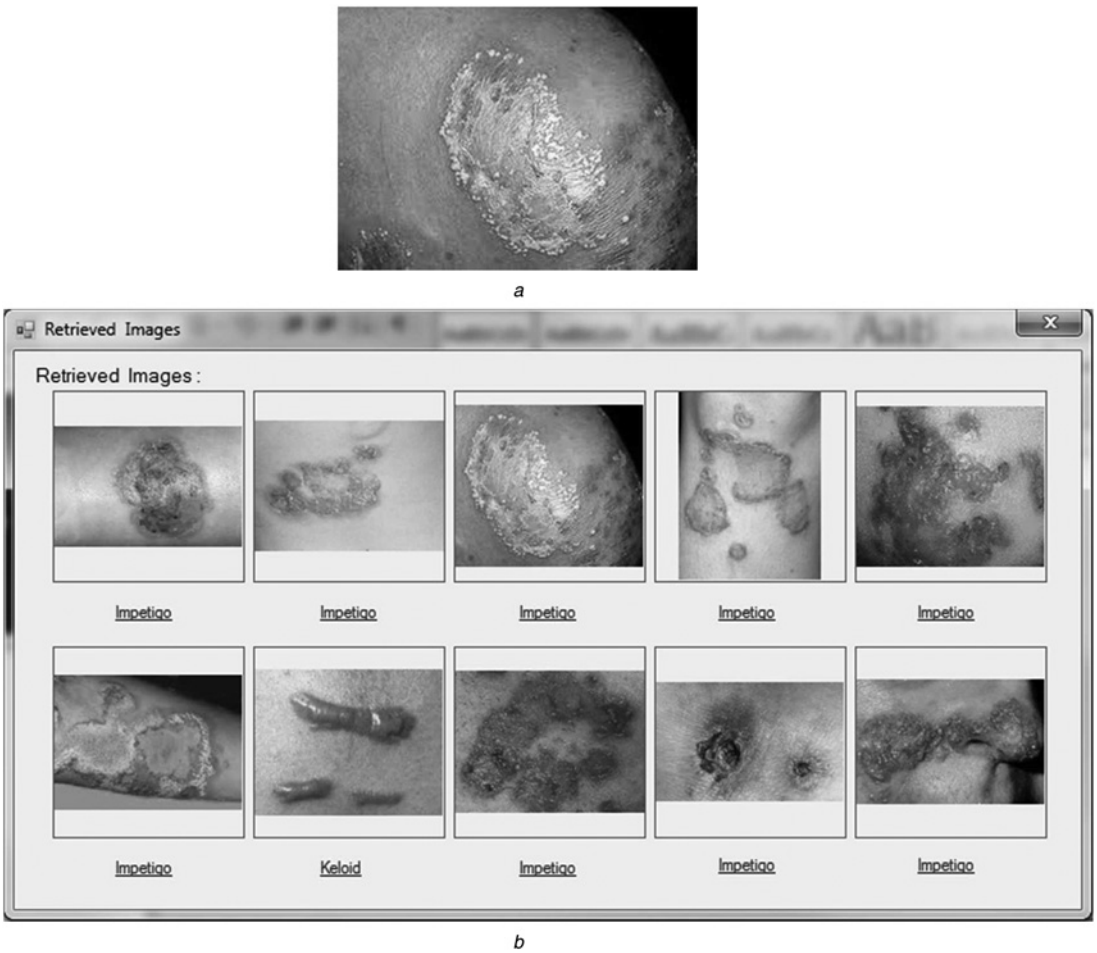

Fig. 8 *Results comparison between our method and earlier works*

a Disease affected sample input: impetigo
b Retrieval result by using fusion of colour and texture feature vectors using proposed work
c Retrieval results of work [33] for query image is equals to impetigo
d Retrieval results of work [34] for query image is equals to impetigo

doi: 10.1049/iet-ipr.2013.0501

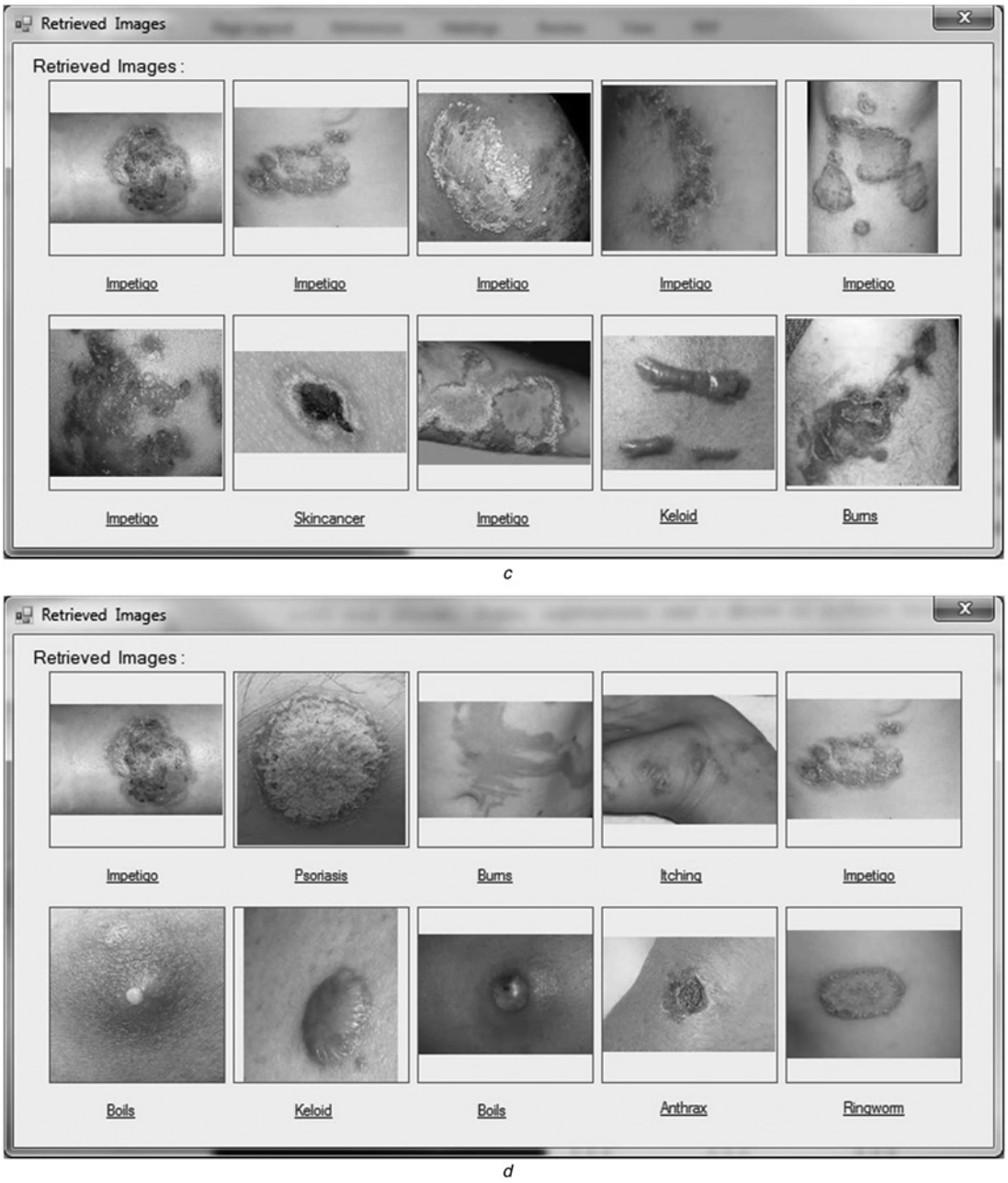

Fig. 8 *Continued*

the validation sample with *k*-folds. The acceptable cost of the tree is met then the change is kept.

The procedure for training process is given below:

Step 1: The training data set *S* with *M* features for *C* class of diseases.
Step 2: The optimal splitting criteria is to be identified in each node based on the GINI index in (26). The node is splitted as the left and right child based on the splitting criteria.
Step 3: For each node Step 2 is applied recursively until one of the following cases:

- Depth of the constructed tree branch has reached the specified maximum value.
- All the samples in the node belong to the same class.

Step 4: Once the tree is built the *K*-fold cross validation is applied for pruning. The misclassification rate is to identify the cost of the tree. Once the required cost is archive the tree has been finalised.

The output of the decision tree has clustered the images into classes to converge the search space efficiently.

3.6 Similarity measure

For similarity measure, we have used Mahalanobis [30], Euclidean [31] and Chebyshev [32] distances and identified that the Euclidean distance measure produced a very good retrieval rate when compared with other distance measures. The statistical performance is given in Table 2.

4 Results and evaluation

We have implemented a fusion strategy colour, texture and shape feature vectors for image retrieval system. We have tested with 20 disease categories, that is, acne, anthrax,

Table 3 Statistical report of proposed method with work [33, 34]

Class	Proposed method				Work [33]				Work [34]			
	Accuracy	Sensitivity	Specificity	*F*-measure	Accuracy	Sensitivity	Specificity	*F*-measure	Accuracy	Sensitivity	Specificity	*F*-measure
1	0.949	0.99	0.988	0.947	0.963	0.800	0.988	0.841	0.835	0.750	0.884	0.853
2	0.962	0.900	0.966	0.818	0.962	0.900	0.999	0.946	0.838	0.780	0.834	0.936
3	0.965	0.600	0.990	0.747	0.947	0.800	0.977	0.800	0.825	0.800	0.851	0.800
4	0.985	0.999	0.990	0.990	0.946	0.990	0.988	0.947	0.762	0.750	0.872	0.957
5	0.938	0.900	0.988	0.900	0.903	0.900	0.988	0.857	0.726	0.800	0.842	0.865
6	0.954	0.990	0.99	0.99	0.892	0.990	0.988	0.947	0.731	0.700	0.925	0.947
7	0.949	0.900	0.988	0.900	0.942	0.800	0.999	0.888	0.867	0.690	0.890	0.891
8	0.968	0.900	0.988	0.942	0.952	0.900	0.988	0.900	0.841	0.710	0.820	0.921
9	0.982	0.990	0.977	0.904	0.937	0.990	0.977	0.904	0.852	0.680	0.820	0.934
10	0.939	0.900	0.988	0.900	0.881	0.900	0.999	0.946	0.782	0.670	0.765	0.953
11	0.934	0.980	0.977	0.921	0.909	0.966	0.966	0.912	0.781	0.740	0.816	0.890
12	0.951	0.970	0.966	0.853	0.938	0.933	0.977	0.812	0.809	0.820	0.819	0.845
13	0.928	0.900	0.955	0.849	0.898	0.900	0.922	0.824	0.743	0.820	0.904	0.809
14	0.952	0.940	0.990	0.793	0.929	0.911	0.900	0.721	0.791	0.780	0.791	0.840
15	0.961	0.700	0.900	0.716	0.937	0.800	0.799	0.699	0.824	0.751	0.876	0.905
16	0.949	0.900	0.922	0.928	0.932	0.899	0.900	0.910	0.819	0.683	0.834	0.889
17	0.957	0.990	0.988	0.946	0.941	0.977	0.966	0.932	0.826	0.724	0.852	0.795
18	0.968	0.980	0.990	0.891	0.956	0.944	0.970	0.875	0.831	0.784	0.849	0.812
19	0.939	0.900	0.922	0.900	0.909	0.900	0.890	0.882	0.784	0.692	0.816	0.791
20	0.946	0.920	0.988	0.923	0.911	0.822	0.977	0.912	0.765	0.721	0.823	0.809

boils, burns, impetigo, itching, keloid, psoriasis, ringworm, skin cancer, hives, shingles, heat rash, staphylococcal folliculitis, pseudononas folliculitis, Cherry angioma, molluscum, eczema, Comedo and Warts are given in Fig. 2. In our database, we have totally 1210 images and all the images are annotated by dermatologists. For training 400 images and testing 810 images are used. The images and the respective feature vectors are stored in database (MS-Access). Database contains the attributes disease name, skin image and its extracted features for each case. The size of feature vector is 66. After applying feature reduction, the size is reduced to 20. The extracted feature vectors are applied to retrieval system and similarity measure will suggest the respective disease category.

In this work, first, we applied level set evolution without re-initialisation [19] technique to detect the lesion borders. We present sample detected lesion borders in various stages as shown in Fig. 5 and the lesion area are fed to input for feature extraction, selected 20 best features which are given to retrieval system and for similarity measure the Euclidean distance was used. The effectiveness of the proposed retrieval system is evaluated on our image database of 1210 lesions, belonging to 20 classes. These graphs justify our choices of best parameters and techniques for our system. Figs. 6 and 7 show the precision/recall curves and sensitivity/specificity obtained using proposed work and earlier works [33, 34]. Our system precision is about 8% higher of their system one. Figs. 8*a–d* show the results comparison between our method and earlier works [33, 34]. The proposed work has a better discrimination power than [33, 34]. The proposed method's retrieval efficiency is based on the specificity and sensitivity. The performances across approaches investigated are illustrated in Tables 3 and 4, Fig. 6 and Fig. 9. Results show that the proposed algorithm produce results that are optimal in performance with other works in terms of precision, recall, sensitivity, *F*-score, specificity and accuracy. During testing phase, out of 810 images, 739 images are correctly retrieved in the respective classes and 71 images are wrongly identified. We achieved 97.25% on specificity and 91.24% on sensitivity. In earlier works, it was only [33] 95.79 and 90.11% and [34] 84.41 and 74.22%.

Table 4 Accuracy report of proposed method with work [33, 34] based on the Euclidean distance

Class	Proposed method accuracy, %	Work [33] accuracy, %	Work [34] accuracy, %
1	94.9	96.3	83.5
2	96.2	96.2	83.8
3	96.5	94.7	82.5
4	98.5	94.6	76.2
5	93.8	90.3	72.6
6	95.4	89.2	73.1
7	94.9	94.2	86.7
8	96.8	95.2	84.1
9	98.2	93.7	85.2
10	93.9	88.1	78.2
11	93.4	90.9	78.1
12	95.1	93.8	80.9
13	92.8	89.8	74.3
14	95.2	92.9	79.1
15	96.1	93.7	82.4
16	94.9	93.2	81.9
17	95.7	94.1	82.6
18	96.8	95.6	83.1
19	93.9	90.9	78.4
20	94.6	91.1	76.5

doi: 10.1049/iet-ipr.2013.0501

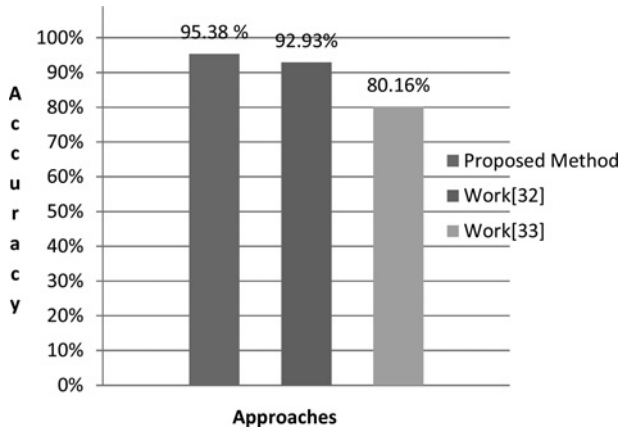

Fig. 9 *Accuracy analysis of proposed method with work [33, 34]*

As the sensitivity (also known as recall rate) describes the fraction of true positives detected out of all existing positives, and the specificity describes the fraction of true negatives out of all existing negatives, this shows that a dermatologist is much less likely to detect a lesion by its outline alone, but the computer program also detects many more lesions.

In summary, our findings support correct diagnosing of dermatology using differences of colour, texture and shape features.

5 Conclusions

We have presented a CBIR system as a diagnostic aid for skin lesion images. We believe that presenting images with known pathology that are visually similar to an image being evaluated may provide intuitive clinical decision support to dermatologists. As exhibited in the experiments, the proposed method outperforms state of art methods in terms of accuracy conditions: illumination and disease. With this it shows the potential to be applied to a range of medical analysis. Our future work is focused on building a better hybrid feature vector to overcome the false positives and false negatives. We plan also to include relevance feedback, which is commonly used in image retrieval, but has not yet been used for medical images.

6 Acknowledgment

The authors thank the DRDO, New Delhi for funding this project.

7 References

1 Müller, H., Michoux, N., Bandon, D., *et al.*: 'A review of content-based image retrieval systems in medical applications-clinical benefits and future directions', *Int. J. Med. Inf.*, 2004, **73**, (1), pp. 1–23
2 Kakumanu, P., Makrogiannis, S., Bourbakis, N.: 'A survey of skin-color modeling and detection methods', *Pattern Recogn.*, 2007, **40**, (3), pp. 1106–1122
3 Cheng, Y.I., Swamisai, R., Umbaugh, S.E., *et al.*: 'Skin lesion classification using relative color features', *Skin Res. Technol.*, 2008, **14**, (1), pp. 53–64
4 Bosman, H.H., Petkov, N., Jonkman, M.F.: 'Comparison of color representations for content-based image retrieval in dermatology', *Skin Res. Technol.*, 2010, **16**, (1), pp. 109–113
5 Claridge, E., Hall, P.N., Keefe, M., *et al.*: 'Shape analysis for classification of malignant melanoma', *J. Biomed. Eng.*, 1992, **14**, (3), pp. 229–234
6 Stoecker, W.V., Moss, R.H.: 'Editorial: digital imaging in dermatology', *Comput. Med. Imaging Graph.*, 1992, **16**, (3), pp. 145–150
7 Celebi, M.E., Iyatomi, H., Schaefer, G., *et al.*: 'Lesion border detection in dermoscopy images', *Comput. Med. Imaging .Graph.*, 2009, **33**, (2), pp. 148–153
8 Wollina, U., Burroni, M., Torricelli, R., *et al.*: 'Digital dermoscopy in clinical practise: a three-centre analysis', *Skin Res. Technol.*, 2007, **13**, (2), pp. 133–142
9 Lee, T.K., Claridge, E.: 'Predictive power of irregular border shapes for malignant melanomas', *Skin Res. Technol.*, 2005, **11**, (1), pp. 1–8
10 Celebi, M.E., Kingravi, H.A., Uddin, B., *et al.*: 'A methodological approach to the classification of dermoscopy images', *Comput. Med. Imaging .Graph.*, 2007, **31**, (6), pp. 362–373
11 Chung, S.M., Wang, Q.: 'Content-based retrieval and data mining of a skin cancer image database'. IEEE Proc., Int. Conf. on Information Technology: Coding and Computing, April 2001, pp. 611–615
12 Celebi, M.E., Aslandogan, Y.A.: 'Content-based image retrieval incorporating models of human perception'. IEEE Proc., Int. Conf. on Information Technology: Coding and Computing, ITCC, April 2004, vol. 2, pp. 241–245
13 Rahman, M.M., Desai, B.C., Bhattacharya, P.: 'Image retrieval-based decision support system for dermatoscopic images'. 19th IEEE Int. Symp. on Computer-Based Medical Systems, CBMS, June 2006, pp. 285–290
14 Dorileo, E.A.G., Frade, M.A., Roselino, A.M., *et al.*: 'Color image processing and content-based image retrieval techniques for the analysis of dermatological lesions'. 30th Annual Int. Conf. of the IEEE Engineering in Medicine and Biology Society, EMBS, August 2008, pp. 1230–1233
15 'Dermnet: the dermatologist's image resource (2007) dermatology image atlas', available at: http://www.dermnet.com/
16 Cohen, B.A., Lehmann, C.U.: 'Dermatlas (2000–2009) dermatology image atlas', available at: http://www.dermatlas.med.jhmi.edu/derm/
17 Timofeev, R.: 'Classification and regression trees (cart) theory and applications'. Master Thesis, Humboldt University, Berlin, 2004
18 Baranidharan, T., Ghosh, D.K.: 'Classification of medical images using fast Hilbert transform and decision tree algorithms', *Int. J. Comput. Sci. Eng.*, 2011, **3**, (4), pp. 1497–1500
19 Li, C., Xu, C., Gui, C., *et al.*: 'Level set evolution without re-initialization: a new variational formulation'. IEEE Computer Society Conf. on Computer Vision and Pattern Recognition, CVPR, June 2005, vol. 1, pp. 430–436
20 Schnabel, J.A.: 'Multi-scale active shape description in medical imaging'. Doctoral dissertation, University College London-University of London, 1998
21 Miller, P., Astley, S.: 'Automated detection of mammographic asymmetry using anatomical features', *Int. J. Pattern Recogn. Artif. Intell.*, 1993, **7**, (6), pp. 1461–1476
22 Graham, R.L.: 'An efficient algorithm for determining the convex hull of a finite planar set', *Inf. Process. Lett.*, 1972, **1**, (4), pp. 132–133
23 Yang, M., Kpalma, K., Ronsin, J.: 'A survey of shape feature extraction techniques, pattern recognition techniques, technology and applications', in Peng-Yeng, Y. (ed.), (I-Tech, Vienna, Austria, 2008), pp.626, ISBN 978-953-7619-24-4
24 Amadasun, M., King, R.: 'Textural features corresponding to textural properties', *IEEE Trans. Syst. Man Cybern.*, 1989, **19**, (5), pp. 1264–1274
25 Jiji, G.W.: 'Colour texture classification for human tissue images', *Appl. Soft Comput.*, 2011, **11**, (2), pp. 1623–1630
26 López, F., Valiente, J.M., Baldrich, R., *et al.*: 'Fast surface grading using color statistics in the CIE Lab space'. Pattern Recognition and Image Analysis, Springer, Berlin, Heidelberg, 2005, pp. 666–673
27 Bianconi, F., Harvey, R., Southam, P.: 'Theoretical and experimental comparison of different approaches for color texture classification', *J. Electron. Imaging*, 2011, **20**, (4), pp. 043006–043006
28 Scott, E.U.: 'Digital image processing and analysis: human and computer vision applications with CVIPtools' (CRC Press, Taylor & Francis Group, Boca Raton, FL, 2011, 2nd edn.), pp. 775–785, 803–810, 820–830
29 Bevington, P.R.: 'Data reduction and error analysis for the physical sciences' (McGraw-Hill, New York, 1969)
30 Dasgupta, S.: 'The evolution of the D^2-statistic of mahalanobis', *Indian J. Pure Appl. Math.*, 1995, **26**, (6), pp. 485–501
31 Fabbri, R., Costa, L.D.F., Torelli, J.C., *et al.*: '2D Euclidean distance transform algorithms: a comparative survey', *ACM Comput. Surv. (CSUR)*, 2008, **40**, (1), p. 2
32 Schoenharl, T.W., Madey, G.: 'Evaluation of measurement techniques for the validation of agent-based simulations against streaming data'. Computational Science – ICCS, Springer, Berlin, Heidelberg, 2008, pp. 6–15
33 Park, S.B., Lee, J.W., Kim, S.K.: 'Content-based image classification using a neural network', *Pattern Recogn. Lett.*, 2004, **25**, (3), pp. 287–300
34 Murthy, V.S.V.S., Vamsidhar, E., Kumar, J.S., *et al.*: 'Content based image retrieval using Hierarchical and K-means clustering techniques', *Int. J. Eng. Sci. Technol.*, 2010, **2**, (3), pp. 209–212